Acta Geochim (2024) 43:354–365
https://doi.org/10.1007/s11631-023-00671-1

ORIGINAL ARTICLE

Experimental study on reactions between alkaline basaltic melt and orthopyroxenes: constraints on the evolution of lithospheric mantle in the North China Craton

Hanqi He[1,2] · Mingliang Wang[3] · Hongfeng Tang[1]

Received: 25 April 2023 / Revised: 14 December 2023 / Accepted: 27 December 2023 / Published online: 23 January 2024

Abstract The experimental results of the reactions between an alkaline basaltic melt and mantle orthopyroxenes under high-temperature and high-pressure conditions of 1300–1400 °C and 2.0–3.0 GPa using a six-anvil apparatus are reported in this paper. The reactions are proposed to simulate the interactions between melts from the asthenospheric mantle and the lithospheric mantle. The starting melt in the experiments was made from the alkaline basalt occurring in Fuxin, Liaoning Province, and the orthopyroxenes were separated from the mantle xenoliths in Damaping, Hebei Province. The results show that clinopyroxenes were formed in all the reactions between the alkaline basaltic melt and orthopyroxenes under the studied P–T conditions. The formation of clinopyroxene in the reaction zone is mainly controlled by dissolution–crystallization, and the chemical compositions of the reacted melt are primarily influenced by the diffusion effect. Temperature is the most important parameter controlling the reactions between the melt and orthopyroxenes, which has a direct impact on the melting of orthopyroxenes and the diffusion of chemical components in the melt. Temperature also directly controls the chemical compositions of the newly formed clinopyroxenes in the reaction zone and the reacted melt. The formation of clinopyroxenes from the reactions between the alkaline basaltic melt and orthopyroxenes can result in an increase of CaO and Al_2O_3 contents in the rocks containing this mineral. Therefore, the reactions between the alkaline basaltic melt from the asthenospheric mantle and orthopyroxenes from the lithospheric mantle can lead to the evolution of lithospheric mantle in the North China Craton from refractory to fertile with relatively high CaO and Al_2O_3 contents. In addition, the reacted melts in some runs were transformed from the starting alkaline basaltic into tholeiitic after reactions, indicating that tholeiitic magma could be generated from alkaline basaltic one via reactions between the latter and orthopyroxene.

Keywords Alkaline basaltic melt · Orthopyroxene · Melt–mineral reaction · High-temperature and high-pressure experiment · Genesis of basalt · Evolution of lithospheric mantle in the North China Craton

1 Introduction

The North China Craton (NCC) in eastern China has been always in a stable state since cratonization at ~ 1.85 Ga (Wu et al. 2008). However, it has become unstable due to the strong influence of multistage tectonism since the Mesozoic because the NCC is located in the region enclosed by the Xingmeng orogenic belt, Qinling–Dabie–Sulu orogenic belt, and Pacific plate. The unstable state of the NCC makes it significantly different from other stable cratons worldwide and therefore has received intensive attention from domestic and foreign geologists for decades. Many case studies (Fan et al. 2000; Xu 2001; Zhou 2006; Zheng et al. 2006a, 2007a; Zhang et al. 2007; Gao et al. 2008, 2009; Wu et al. 2008; Lu 2010) have shown that, with its transition from stable to unstable, the lithospheric mantle of the NCC has undergone an evolution from a cratonic and refractory

✉ Hongfeng Tang
tanghongfeng@mail.gyig.ac.cn

[1] Key Laboratory for High Temperature and High Pressure Study of the Earth's Interior, Institute of Geochemistry, Chinese Academy of Sciences, Guiyang 550081, China

[2] University of Chinese Academy of Sciences, Beijing 100049, China

[3] School of Resource and Civil Engineering, Suzhou University, Suzhou 234000, Anhui, China

mantle dominated by harzburgite to an oceanic and fertile one dominated by lherzolite.

The mechanism of the evolution in the lithospheric mantle of the NCC is still debated thus far. Some previous case studies (e.g. Zhang 2006, 2009) have suggested that the interactions between peridotites and melts may be an important way of modifying the lithospheric mantle in the NCC. The cratonic lithospheric mantle lies spatially between the continental crust and asthenosphere. Thus, its evolution is undoubtedly closely related to the latter two tectonic units. On the one hand, melting of the continental crust entering the mantle through subduction or delamination can result in the formation of high-Si melts, which can react with minerals or peridotites during their migration within the lithospheric mantle. On the other hand, melts such as tholeiitic, alkaline basaltic, and carbonatitic melts originated from the asthenosphere can react with minerals or peridotites when they ascend through the lithospheric mantle.

Experimental simulation under high-temperature and high-pressure conditions is an effective way to verify the mechanism of the evolution in the lithospheric mantle of the NCC. Some experimental studies on reactions between melts and rocks or minerals under high-temperature and high-pressure conditions have been carried out, and the following main conclusive insights obtained. (1) The main mineral formed in the interaction between Si-rich melt and mantle olivine (Wang and Tang 2013) or peridotite (Wang et al. 2019) is orthopyroxene, and the residual melt after reaction has increased MgO content and Mg# value, providing direct evidence for the occurrence of high-Mg andesite and adakite in the NCC. (2) Olivine and clinopyroxene can be formed in the interaction between Si-poor melt and mantle peridotite under lower and higher pressure conditions, respectively (Kelemen et al. 1990; Morgan and Liang 2003, 2005). (3) Clinopyroxene is newly formed in the interaction between tholeiitic basaltic melt and mantle peridotite (Yaxley and Green 1998; Mallik and Dasgupta 2012) or orthopyroxene (Zang et al. 2021). (4) The interaction between melt and peridotite is virtually between melt and minerals in peridotite, and is mainly affected by constituent minerals in peridotite (Wang et al. 2013) and by melt composition (Wang et al. 2019). These studies provide good direct evidence for elucidating the genesis of some characteristic rocks but are insufficient to constrain the evolution of the lithospheric mantle in the NCC. Recently, the experimental results of the reactions between eclogite-derived subalkaline melt and lherzolite (Wang et al. 2020), and between Ca-rich carbonatite melt and peridotite (Wang et al. 2022) were reported. The results are of great significance for understanding the lithospheric mantle modification beneath the NCC. However, except for subalkaline and carbonate melts, the asthenosphere-derived alkaline melt (Zou 2010) also has an impact on the evolution of the lithospheric mantle in the NCC. In this paper, our experimental results on the reaction of an alkaline basaltic melt with orthopyroxenes from a mantle peridotite at 1300–1400 °C and 2.0–3.0 GPa on a six-anvil apparatus are reported. The results provide additional direct evidence for the mechanism of melt–rock interaction leading to the evolution of lithospheric mantle in the NCC from refractory to fertile.

2 Experimental and analytical methods

2.1 Starting materials

The starting materials used in our experiments include the alkaline basalt occurring in Fuxin, Liaoning Province and orthopyroxenes separated from a mantle xenolith discovered in Damaping, Hebei Province. A previous study (Zhang and Zheng 2003) has suggested that the alkaline basalt was the product of undifferentiated and uncontaminated primitive magma originated from a depleted asthenospheric mantle. Therefore, it can be considered as the starting material simulating the melt from asthenosphere. The homogeneous alkaline basaltic glass was prepared by crushing chips of the fresh alkaline basalt, ultrasonic washing with distilled water and ethanol, grinding manually in an agate mortar to a ~200 mesh powder, melting three times in a Fe-saturated Pt crucible at 1500 °C and 1 atm for an hour, and quenching. The pure orthopyroxene grains were prepared by crushing the mantle xenolith to ~20 mesh separates, handpicking under a binocular microscope, and ultrasonic washing with deionized water and ethanol. The major-element compositions of the orthopyroxene and glass used in the experiments are listed in Table 1.

Table 1 Major-element compositions (wt.%) of the starting materials

	SiO_2	TiO_2	Al_2O_3	Cr_2O_3	FeO*	Fe_2O_3*	MnO	MgO	CaO	Na_2O	K_2O	P_2O_5	Total
Orthopyroxene	54.46	0.17	4.38	0.35	6.30		0.11	33.49	0.63	0.17			100.07
Glass	45.24	2.97	15.17			12.24	0.17	8.49	10.15	3.58	1.33	0.64	

(1) FeO* and Fe_2O_3* are the total iron expressed as FeO and Fe_2O_3, respectively. (2) The data of the glass are recalculated to 100 wt.% anhydrous from primary XRF result

2.2 Experimental conditions and procedure

The purpose of the experiments is to explore the reaction between the melt and orthopyroxene. For this purpose, it is necessary to completely melt the glass while orthopyroxene grains are stable as solid loaded in the capsule. Based on previous experiments on the melting of alkaline basalt (Bao et al. 2011) and orthopyroxene (Wyllie 1979), combined with the possible depth of melt-rock reactions in the lithospheric mantle of the NCC, the experimental temperature and pressure in this study were set at 1300–1400 °C and 2.0–3.0 GPa. The detailed experimental P–T conditions are given in Table 2.

All the reaction experiments were performed using the YJ-3000t six-anvil apparatus equipped at the Key Laboratory for High Temperature and High Pressure Study of the Earth's Interior of the Institute of Geochemistry, Chinese Academy of Sciences. The starting materials, alkaline basaltic glass powder and orthopyroxene, were loaded using an interbedded manner in a Pt capsule with a graphite inner capsule. The Pt capsule has an inner diameter of 6 mm and a length of 6 mm. The loaded materials and the wall of the Pt capsule were separated by graphite, which can prevent Fe loss (Sisson and Grove 1993). The loaded Pt capsule was filled in a thin-walled Al_2O_3 sleeve, and these two parts then were placed in a graphite heater, which was plugged by a calcined pyrophyllite cylinder at both ends. The detailed sample assemblage for the experiments is illustrated in Fig. 1. Based on the weights of the starting materials loaded in the capsule, the proportion of melt relative to orthopyroxene in each run was determined. The temperature was measured and monitored using $PtRh_6$–$PtRh_{30}$ thermocouples, and accurate to 5 °C. The pressure was accurate to 0.1 GPa. In a single run, the pressure was first raised to the desired value, and then the temperature was increased at a rate of 50 °C/min to the desired value. Finally, the experiment was held at the desired temperature and pressure conditions. After the designed duration, the experimental charge was quenched by turning the power off, and then the run product was removed carefully from the capsule and mounted in epoxy, which was polished for observation and electron microprobe analysis.

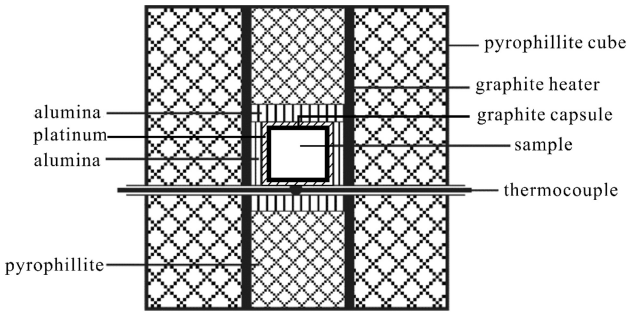

Fig. 1 Sketch map showing the sample assemblage for the experiments in this study

2.3 Sample analysis

The chemical composition of the alkaline basalt was analysed on an Axios (PW4400) X-ray fluorescence (XRF) spectrometer at the State Key Laboratory of Ore Deposit Geochemistry (SKLODG), Institute of Geochemistry, Chinese Academy of Sciences (IGCAS). The chemical compositions of the starting orthopyroxene and run products were determined on a JXA8530F-plus field emission electron microprobe at SKLODG. The accelerating potential was 15 kV and the beam current was 10 nA. The backscattered electron (BSE) images of the run products were obtained by a Scios scanning electron microscopy (SEM) at the Center for Lunar and Planetary Sciences of IGCAS with an accelerating potential of 15 or 25 kV.

Table 2 Experimental conditions and phase assemblages of the run products

Run No	Temperature (°C)	Pressure (GPa)	Duration (h)	Gl:Opx	Phase assemblage
hq-29	1300	2.0	48	2:1	Gl + Opx + Cpx + Grt
hq-12	1350	3.0	8	2:1	Gl + Opx + Cpx + Grt
hq-14	1350	3.0	20	1:1	Gl + Opx + Cpx + Grt
hq-15	1350	3.0	8	1:1	Gl + Opx + Cpx + Grt
hq-19	1350	2.0	8	3:1	Gl + Opx + Cpx + Grt
hq-26	1350	3.0	72	2:1	Gl + Opx + Cpx
hq-28	1350	3.0	72	1:1	Gl + Opx + Cpx + Grt
hq-31	1350	2.0	48	2:1	Gl + Opx + Cpx
hq-30	1400	2.0	16	2:1	Gl + Opx + Cpx
hq-33	1400	2.0	72	2:1	Gl + Opx + Cpx

Phase abbreviation Gl = melt, Opx = orthopyroxene, Cpx = clinopyxene, Grt = garnet. Gl and Opx are the reacted starting materials, and Cpx and Grt are the newly formed minerals. Gl:Opx is the mass ratio of the starting melt powder to orthopyroxene loaded in the Pt capsule for each experiment

3 Experimental results

The phase assemblages of the run products are given in Table 2. The representative BSE images are illustrated in Fig. 2. The chemical compositions of the run products are listed in Table 3. The results show that three phases, melt, orthopyroxene and clinopyroxene, were obtained in all ten successful experiments. As shown in Fig. 2, the orthopyroxene was dissolved and eroded, forming an uneven, embay-like dissolution rim. Clinopyroxene is produced in bands around orthopyroxene with a bandwidth of about 100–200 μm and sometimes euhedral crystal edge can be observed (Fig. 2D). Melt and orthopyroxene are the residual phases after reaction and hence named reacted melt and reacted orthopyroxene, respectively, whilst clinopyroxene is newly formed through reaction and developed in the reaction zone between melt and orthopyroxene (Fig. 2). In addition, garnet was also newly formed in some runs (Fig. 2A, B), which is consistent with garnet occurrence in the basaltic system reported by Green (1982). Garnet grains are distributed both in the reacted melt and the reaction zones associated with clinopyroxene, and are granular in shape and generally 10–40 μm in diameter.

The major-element compositions of the reacted melt are generally homogeneous (Table 3), and mainly exhibit two kinds of characteristics. One kind is SiO_2 and MgO, which are significantly higher in the starting orthopyroxene than in the starting melt (Table 1). After the reaction, the SiO_2 and MgO concentrations of the reacted melt are both higher than those of the starting melt, and the extent of concentration raise of these two components in the reacted melt increases with increasing reaction temperature. At the same ratio of melt/orthopyroxene (2:1), the SiO_2 and MgO concentrations of the reacted melt show a certain degree of linear positive correlation with reaction temperature (Fig. 3A, E). The others, in contrast, are TiO_2, Al_2O_3, FeO, CaO, and Na_2O, which are lower in the starting orthopyroxene than in the starting melt (Table 1). All these components in the reacted melt have basically lower concentrations than in the starting melt, and except for Al_2O_3, the extent of concentration reduction of these components in the reacted melt increases with increasing reaction temperature, resulting in a certain degree of linear negative correlation (Fig. 3B, D, F) between the concentrations of these components in the reacted melt and temperature at melt/orthopyroxene ratio of 2:1. No linear relationship between the Al_2O_3 concentration of the reacted melt and reaction temperature at melt/orthopyroxene ratio of 2:1 is exhibited (Fig. 3C). The reason is due to no crystallization of garnet, an Al-rich mineral, at high temperatures (Table 2), which leads to the extent

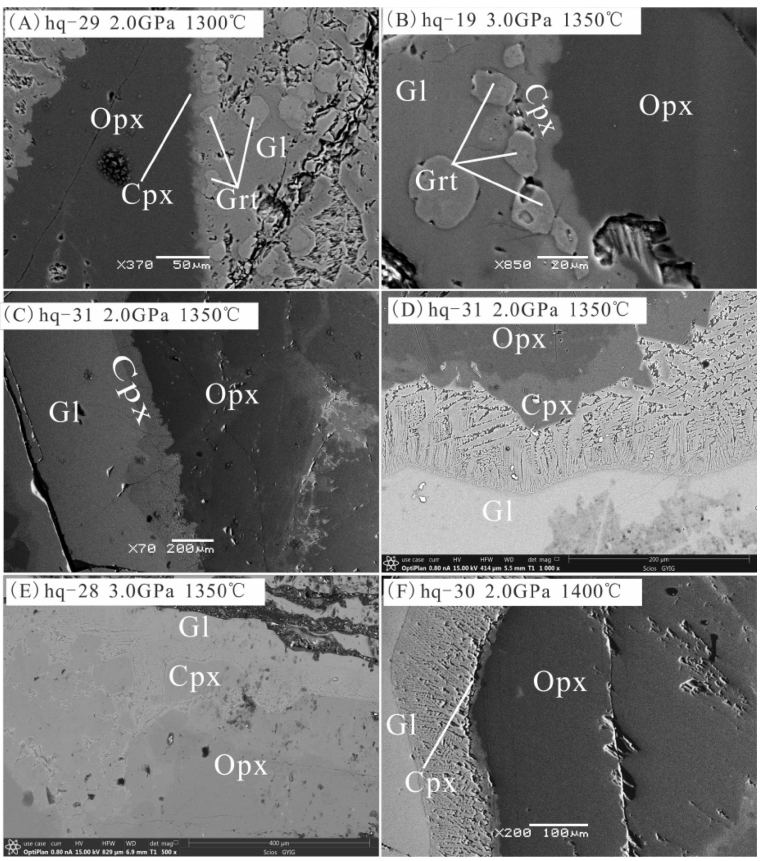

Fig. 2 Representative BSE images of run products. Newly formed clinopyroxene occurring in bands around orthopyroxene. It is worth noting that the euhedral crystal edge of clinopyroxene can be observed in this figure D, enlargement of the clinopyroxene band in this figure C

Table 3 Major-element compositions (wt.%) of the run products

Run No	hq-29	hq-12	hq-14	hq-15	hq-19	hq-26	hq-28	hq-31	hq-30	hq-33
T (°C)	1300	1350	1350	1350	1350	1350	1350	1350	1400	1400
P (GPa)	2.0	3.0	3.0	3.0	3.0	3.0	3.0	2.0	2.0	2.0
Gl:Opx	2:1	2:1	1:1	1:1	3:1	2:1	1:1	2:1	2:1	2:1
N	4	3	3	9	4	11	3	5	6	3
Reacted melt										
SiO_2	45.50 (0.31)	46.18 (0.88)	46.95 (0.30)	48.60 (2.98)	44.88 (1.01)	46.22 (0.15)	46.84 (0.55)	46.16 (0.19)	46.50 (0.68)	46.40 (0.72)
TiO_2	4.18 (0.13)	1.92 (0.09)	2.03 (0.24)	2.30 (0.26)	2.51 (0.67)	2.89 (0.04)	2.90 (0.11)	3.03 (0.06)	2.70 (0.08)	2.50 (0.30)
Al_2O_3	14.84 (0.33)	11.94 (1.00)	11.90 (0.50)	12.65 (0.62)	14.52 (1.18)	14.09 (0.19)	14.44 (0.29)	13.94 (0.16)	15.09 (0.31)	13.70 (0.48)
FeO	12.09 (0.09)	10.12 (1.68)	10.08 (0.90)	8.83 (1.02)	11.14 (0.50)	11.22 (0.14)	11.49 (0.06)	11.61 (0.03)	11.36 (0.35)	11.14 (0.39)
MnO	0.17 (0.01)	0.22 (0.04)	0.21 (0.02)	0.20 (0.02)	0.24 (0.02)	0.18 (0.02)	0.18 (0.02)	0.17 (0.01)	0.19 (0.02)	0.21 (0.02)
MgO	7.14 (0.05)	16.49 (0.38)	15.76 (0.38)	14.55 (0.66)	12.21 (2.29)	11.98 (0.47)	10.79 (0.12)	11.55 (0.16)	10.04 (1.13)	13.48 (0.35)
CaO	7.62 (0.07)	11.12 (1.78)	11.12 (0.50)	10.87 (0.73)	11.25 (0.85)	7.78 (0.19)	7.47 (0.02)	7.34 (0.07)	8.58 (0.37)	9.97 (0.22)
Na_2O	5.90 (0.25)	1.92 (0.73)	1.85 (0.12)	1.77 (0.09)	2.28 (0.58)	3.57 (0.24)	3.71 (0.19)	3.90 (0.12)	3.75 (0.54)	2.27 (0.23)
K_2O	1.75 (0.02)	0.02 (0.02)	0.02 (0.01)	0.02 (0.01)	0.44 (0.65)	1.38 (0.13)	1.49 (0.02)	1.59 (0.02)	1.19 (0.28)	0.06 (0.04)
P_2O_5	0.82 (0.05)	0.07 (0.05)	0.07 (0.06)	0.21 (0.08)	0.52 (0.06)	0.67 (0.06)	0.70 (0.04)	0.72 (0.04)	0.60 (0.60)	0.28 (0.09)
σ	23.4	1.2	0.9	0.6	3.9	7.6	7.0	9.5	7.0	1.6
n	5	4	9	3	6	4	5	5	5	11
Reacted orthopyroxene										
SiO_2	54.42 (0.34)	53.88 (1.52)	53.07 (0.75)	52.89 (0.24)	54.47 (0.69)	53.82 (0.23)	55.02 (0.57)	54.96 (0.64)	54.38 (0.30)	53.96 (0.77)
TiO_2	0.09 (0.02)	0.14 (0.08)	0.16 (0.06)	0.08 (0.02)	0.06 (0.02)	0.08 (0.03)	0.13 (0.03)	0.17 (0.11)	0.10 (0.01)	0.18 (0.07)
Al_2O_3	4.10 (0.25)	4.25 (0.30)	4.36 (0.34)	3.85 (0.20)	3.68 (0.36)	4.18 (0.13)	4.15 (0.26)	4.60 (0.30)	3.95 (0.09)	5.19 (0.89)
Cr_2O_3	0.26 (0.04)	0.26 (0.06)	0.21 (0.03)	0.25 (0.03)	0.22 (0.05)	0.27 (0.01)	0.27 (0.02)	0.26 (0.02)	0.24 (0.03)	0.32 (0.09)
FeO	7.76 (0.88)	7.50 (0.09)	8.22 (0.89)	7.51 (0.09)	7.41 (0.10)	7.36 (0.08)	7.55 (0.14)	7.67 (0.39)	7.24 (0.09)	8.21 (0.93)
MnO	0.16 (0.01)	0.14 (0.01)	0.16 (0.02)	0.15 (0.01)	0.15 (0.01)	0.16 (0.01)	0.14 (0.01)	0.16 (0.01)	0.14 (0.01)	0.16 (0.02)
MgO	33.26 (1.04)	32.98 (0.77)	32.38 (1.33)	33.16 (0.06)	34.38 (0.14)	33.87 (0.49)	32.69 (0.53)	33.92 (1.18)	34.11 (0.39)	33.00 (1.96)
CaO	0.47 (0.11)	0.57 (0.22)	0.93 (0.36)	0.43 (0.02)	0.40 (0.05)	0.52 (0.07)	0.54 (0.13)	0.75 (0.41)	0.45 (0.06)	1.24 (0.70)
Na_2O	0.12 (0.07)	0.59 (0.40)	0.18 (0.08)	0.07 (0.03)	0.09 (0.02)	0.14 (0.04)	0.14 (0.05)	0.17 (0.11)	0.13 (0.03)	0.50 (0.68)
Total	100.64	100.31	99.67	98.39	100.86	100.40	100.63	102.66	100.74	102.76
n	4	3	5	5	7	6	3	5	4	3
Clinopyroxene										
SiO_2	51.10 (1.30)	51.59 (0.54)	50.70 (0.79)	54.18 (0.41)	47.70 (0.53)	47.90 (1.18)	48.28 (3.03)	46.46 (0.70)	51.03 (1.23)	51.39 (0.37)
TiO_2	1.06 (0.17)	0.65 (0.02)	0.72 (0.08)	0.82 (0.30)	0.75 (0.09)	2.74 (0.61)	1.94 (1.12)	2.70 (0.42)	0.77 (0.20)	0.56 (0.01)
Al_2O_3	9.47 (1.11)	7.89 (0.46)	8.39 (0.77)	7.54 (0.55)	10.97 (0.87)	12.52 (0.65)	11.90 (2.34)	12.86 (0.46)	9.69 (0.81)	8.70 (0.14)
Cr_2O_3	0.22 (0.05)	0.39 (0.20)	0.29 (0.02)	0.28 (0.03)	0.56 (0.11)	0.08 (0.03)	0.13 (0.14)	0.08 (0.05)	0.36 (0.09)	0.29 (0.04)
FeO	7.90 (0.22)	7.53 (0.89)	7.13 (0.50)	5.63 (0.37)	6.04 (0.34)	8.08 (0.48)	9.25 (2.49)	10.57 (0.56)	7.98 (0.90)	7.61 (0.11)
MnO	0.17 (0.03)	0.20 (0.05)	0.18 (0.02)	0.16 (0.02)	0.15 (0.01)	0.19 (0.02)	0.20 (0.03)	0.18 (0.02)	0.19 (0.02)	0.18 (0.01)

Table 3 (continued)

n	4	3	5	5	7	6	3	5	4	3
MgO	15.07 (1.64)	19.54 (1.55)	17.50 (2.12)	17.17 (1.45)	14.64 (0.97)	15.58 (1.68)	15.45 (1.59)	16.37 (1.20)	18.67 (0.92)	19.54 (0.11)
CaO	13.18 (1.02)	10.90 (1.94)	12.84 (1.76)	12.03 (1.20)	15.51 (0.80)	10.06 (1.05)	10.92 (2.85)	9.10 (0.22)	10.61 (0.75)	11.42 (0.12)
Na_2O	2.52 (0.29)	1.92 (0.28)	1.85 (0.28)	1.60 (0.36)	2.03 (0.18)	1.70 (0.37)	1.83 (0.34)	1.96 (0.19)	1.67 (0.20)	1.50 (0.07)
Total	100.69	100.61	99.60	99.41	98.35	98.85	99.90	100.28	100.97	101.19

n	7	3	5	5	5	5
Garnet						
SiO_2	40.82 (1.02)	40.39 (0.45)	39.84 (0.28)	41.17 (0.56)	39.55 (0.59)	41.59 (0.50)
TiO_2	0.87 (0.09)	0.62 (0.03)	0.76 (0.09)	0.79 (0.09)	0.88 (0.24)	0.64 (0.06)
Al_2O_3	22.63 (0.70)	23.47 (0.22)	22.74 (0.30)	22.03 (0.39)	22.33 (0.54)	23.96 (0.19)
Cr_2O_3	0.18 (0.03)	0.32 (0.02)	0.28 (0.07)	0.46 (0.11)	0.26 (0.03)	0.29 (0.03)
FeO	13.56 (0.61)	11.19 (0.30)	12.61 (0.53)	10.73 (0.93)	12.77 (0.49)	11.63 (0.52)
MnO	0.36 (0.03)	0.33 (0.01)	0.39 (0.03)	0.30 (0.03)	0.45 (0.07)	0.34 (0.03)
MgO	16.19 (0.42)	18.86 (0.27)	15.95 (0.53)	17.13 (0.94)	15.99 (0.44)	17.00 (0.43)
CaO	6.15 (0.55)	5.70 (0.15)	6.77 (0.38)	5.87 (0.50)	6.94 (0.12)	5.85 (0.54)
Na_2O	0.20 (0.22)	0.10 (0.03)	0.11 (0.06)	0.12 (0.05)	0.13 (0.04)	0.08 (0.03)
Total	100.96	100.98	99.45	98.60	99.30	101.38

σ (Rittmann index) = $(Na_2O + K_2O)^2/(SiO_2-43)$

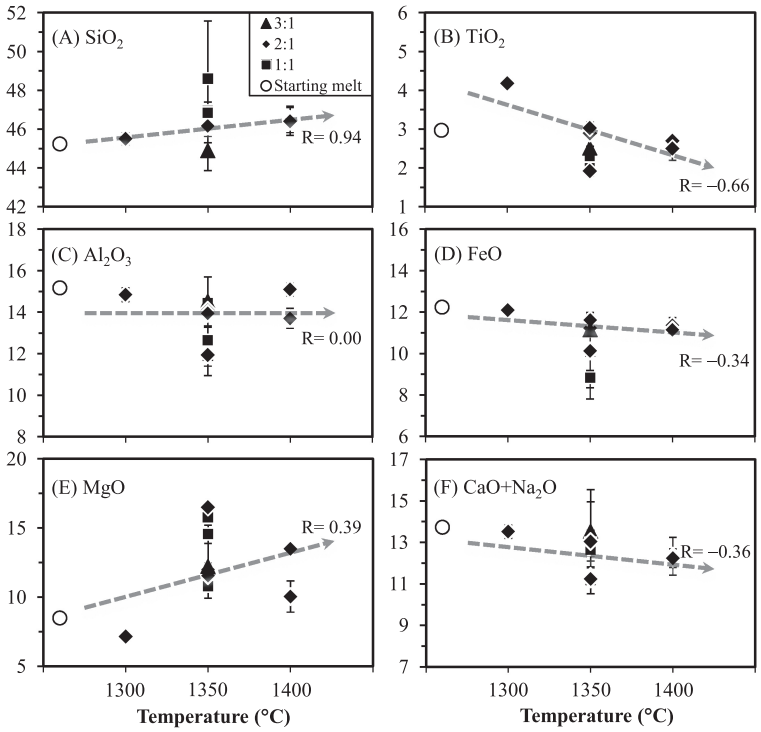

Fig. 3 Relations of SiO_2, TiO_2, Al_2O_3, FeO, MgO, and $CaO + Na_2O$ contents in the reacted melts with temperature and melt ratio. The melt/orthopyroxene ratios of 3:1, 2:1, and 1:1 are represented. The dashed lines with arrow and linear correlation coefficients (R) are the relations between the oxide contents in the reacted melt and temperature at the same melt/orthopyroxene ratio of 2:1. See the text for details

of concentration reduction of Al_2O_3 in the reacted melt not increasing with increasing reaction temperature. It is worth noting that the SiO_2 content of the reacted melt is low and very close to the starting melt at a melt/orthopyroxene ratio of 3:1, significantly higher than that of the starting melt at 1:1, and between the two aforementioned cases at 2:1. In addition, at the same melt/orthopyroxene ratio of 2:1 and temperature of 1350 °C but different pressures, 2.0 GPa

(hq-31) and 3.0 GPa (hq-12, -26), the SiO_2 contents of the reacted melts are consistent and close to that of the starting melt (Table 3), suggesting that pressure has no impact on the SiO_2 content of the reacted melt.

The compositions of the reacted orthopyroxene in all ten experiments (Table 3) are consistent with that of the starting orthopyroxene (Table 1), and the reacted orthopyroxenes are plotted at nearly the same position as the starting orthopyroxene in the classification diagram of En ($Mg_2Si_2O_6$)–Wo ($Ca_2Si_2O_6$)–Fs ($Fe_2Si_2O_6$) (Fig. 4). Therefore, the orthopyroxenes have no obvious modification of the major-element compositions in the reactions at different melt ratios, temperatures, and pressures.

The SiO_2 content of newly formed clinopyroxenes is in the range of 46.46–54.18 wt%; the contents of MgO and CaO are in the ranges of 14.64–19.54 wt% and 9.10–15.51 wt%, respectively. Their En is in the range of 50.2–61.8 %, Wo in the range of 22.7–38.2 %, and Fs in the range of 10.9–20.6 %. In the classification diagram of En–Wo–Fs (Fig. 4), all the clinopyroxenes belong to augite, and most of them are plotted in the range defined by clinopyroxenes from the mantle lherzolites and pyroxenites in the NCC, but there is a certain deviation from the range defined by 95 % of mantle clinopyroxenes.

The newly formed garnets have relatively uniform compositions (Table 3). Their components at different melt ratios, temperatures and pressures are consistent. The components of pyrope, grossular, and almandite + spessartite for these garnets are approximately 60%, 15%, and 25%, respectively. Based on the occurrence of garnet in melts near and far from the reaction zone (Fig. 2) and the homogeneity of chemical composition, it can be determined that the garnets were directly crystallized from the alkaline basaltic melt.

As shown in BSE images (Fig. 2), all newly formed minerals and reacted melts in the run products have no zoning.

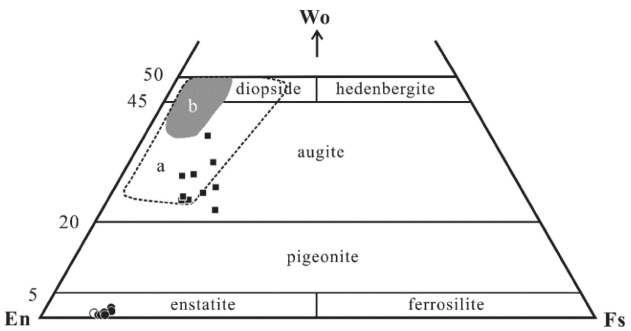

Fig. 4 Classification diagram of En ($Mg_2Si_2O_6$)–Wo ($Ca_2Si_2O_6$)–Fs ($Fe_2Si_2O_6$) for pyroxene. Circle–starting orthopyroxene, filled circle–reacted orthopyroxene, filled square–newly formed clinopyroxene. a–range defined by clinopyroxenes from the mantle lherzolites and pyroxenes in the NCC, b–range defined by 95% of mantle clinopyroxenes, and data are from Liu et al. (2010), Sun et al. (2012), Xiao et al. (2010; 2015), Yu (2009) and Zheng et al. (2000, 2005, 2006b, 2007b)

This indicates that chemical equilibrium had been probably achieved in our runs. Clinopyroxene and garnet coexist in six products (Table 2) among ten runs. The estimated temperatures of four runs by using the average compositions of clinopyroxene and garnet, and applying the geothermometer of Ravna (2000), do not differ by more than 50 °C from the desired temperatures. In particular, the estimated temperature (1272 °C) for run hq-29 with the lowest desired temperature in this study is consistent with the desired temperature (1300 °C). Therefore, it can be considered that our runs like those in Zang et al. (2021) should achieve or approach chemical equilibrium between newly formed minerals (clinopyroxene and garnet) or between these two minerals and reacted melts.

4 Discussion

4.1 Reaction mechanism and influencing factors

It is generally believed that there are two reaction mechanisms between minerals and melts, namely, diffusion and dissolution–crystalliscrystallizationn refers to that the elements between melts and minerals producing different chemical potentials due to the concentration difference, and the elements migrate under the drive of chemical potential (Liang et al. 1996; Liang 1999, 2000, 2010). Dissolution–crystallization refers to that the mineral lattice is destructed under the effect of the melt, whilst the mineral in contact with the melt is melted and mixed with the melt to form a mixed melt in the reaction zone. When certain components in the mixed melt reach supersaturation, they crystallize in the form of new mineral(s).

In this study, the reacted orthopyroxenes are homogenous and have almost the same major-element compositions as the starting orthopyroxene. Therefore, no significant diffusion occurred between melt and orthopyroxene and within orthopyroxene as well in the reactions. In the reaction zone, the melted orthopyroxene was mixed with the starting melt to form a mixed melt with significantly higher MgO and slightly higher SiO_2 contents than the starting melt. The mixed melt also has higher CaO, Al_2O_3, and Na_2O contents than the melted components around the starting orthopyroxene. The supersaturation of the abovementioned components in the mixed melt resulted in the crystallization of clinopyroxenes around the orthopyroxene (Fig. 2).

With increasing temperatures, the melting degree of the orthopyroxene and the amount of MgO added into the mixed melt are increased, resulting in En and Wo components of the newly formed clinopyroxenes, inconsistent with the clinopyroxenes formed in experiments of Yaxley and Green (1998) and Zang et al. (2021), being positively and

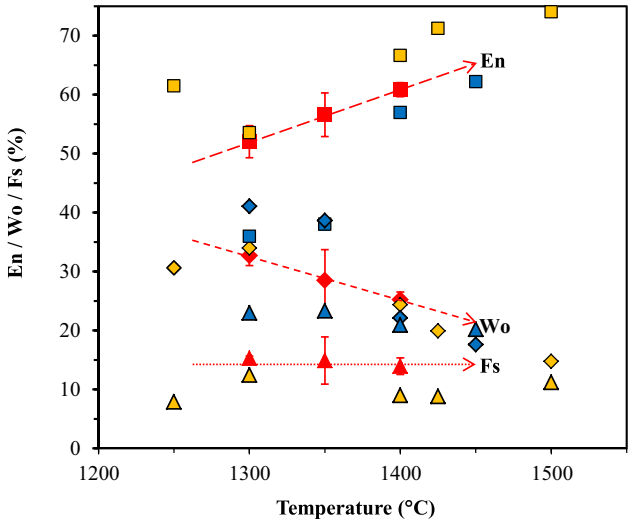

Fig. 5 En/Wo/Fs of the newly formed clinopyroxenes versus temperature. The red symbols are the data in this study, the average values of all newly formed clinopyroxenes at each temperature, and the linear trend of each end-member component is represented by a dashed line. The yellow and blue symbols are the data from Yaxley and Green (1998) and Zang et al. (2021) for comparison, respectively. In general, En (square) and Wo (diamond) are positively and negatively correlated with temperature, respectively, but Fs (triangle) has no obvious correlation with temperature

negatively correlated with temperature, respectively (Fig. 5). The increase of En and decrease of Wo in the newly formed clinopyroxene are due to the dilution effect.

The chemical composition of the reacted melt in each experiment is generally homogenous, and the MgO content of the reacted melt increases significantly compared to the starting melt in the experiments at 1350 and 1400 °C (Table 3). Therefore, there should be a diffusion effect in the melt. This mechanism diffuses the remaining MgO from the melted orthopyroxene into the reacted melt, after meeting the requirements of clinopyroxene crystallization. In the experiment at 1300 °C (hq-29), the MgO content in the reacted melt did not increase. This may be because total MgO from the melted orthopyroxene was consumed during the crystallization of clinopyroxene, or even not enough to meet this crystallization and the MgO in the melt diffused backward to the reaction zone. The probable reasons for the decrease in CaO, Al_2O_3, FeO, and Na_2O contents in the reacted melt are twofold: (1) the melted orthopyroxene diffused into and diluted the melt, and (2) these components in the starting melt diffused and concentrated to the mixed melt in the reaction zone to facilitate the crystallization of clinopyroxene. Both of these possibilities indicate the presence of diffusion in the melt. Based on the chemical compositions of the minerals in run products, the reaction equations can be expressed. The following is the reaction equation for run hq-33 as an example.

$$
\begin{aligned}
&2\left(Mg_{0.9}Fe^{2+}_{0.1}\right)\left(Mg_{0.8}Fe^{3+}_{0.1}Fe^{2+}_{0.1}\right)\\
&\left[\left(Si_{1.9}Al_{0.1}\right)O_6\right](starting Opx)+0.4CaO\cdot 0.2Al_2O_3\cdot\\
&0.05Na_2O(from\ starting\ melt)=\left(Ca_{0.4}Mg_{0.4}Fe^{2+}_{0.1}Na_{0.1}\right)\\
&\left(Mg_{0.6}Al_{0.2}Fe^{3+}_{0.1}Fe^{2+}_{0.1}\right)\left[\left(Si_{1.8}Al_{0.2}\right)O_6\right](newly\ formed\ Cpx)\\
&+\left(Mg_{0.9}Fe^{2+}_{0.1}\right)\left(Mg_{0.8}Fe^{3+}_{0.2}\right)\left[\left(Si_{1.8}Al_{0.2}\right)O_6\right](reacted\ Opx)\\
&+0.7MgO\cdot 0.2SiO_2(to\ reacted\ melt)
\end{aligned}
$$

It can be seen from this equation that significant differences in constituents between the starting orthopyroxene and the starting melt not only promote the reaction, but also provide CaO, Al_2O_3, and Na_2O from the starting melt for the formation of clinopyroxene, and lead to increases in MgO and SiO_2 in the reacted melt as well.

Temperature is a key factor affecting the melting of orthopyroxene and diffusion in the melt. The experimental results in this paper fully demonstrate the important control of temperature on the reactions between melt and orthopyroxene. In addition, the ratio of melt to orthopyroxene has certain constraints on the chemical composition of the reacted melt (Fig. 3). From the experimental results of Run Nos hq-12, -26, and -31, there is no significant effect of pressure on the melt–orthopyroxene reaction. However, whether and how pressure affects the reaction requires further experiments carried out under higher pressure and a wider pressure range.

4.2 Constraints on the evolution of lithospheric mantle in the NCC

From many previous case studies on the mantle xenoliths, it is suggested that the lithospheric mantle of the NCC has been transformed from a refractory mantle to fertile one during the Mesozoic and Cenozoic (Wu et al. 2008; Zhang 2009; Zheng 2009). Although the mechanism of this transformation is still controversial, the melt–rock reaction that occurred in the lithospheric mantle of the NCC is an important mechanism (Zhang 2006, 2009). It has been found that the refractory lithospheric mantle is mainly composed of harzburgite (Fan et al. 2000), while the fertile lithospheric mantle after the transformation is primarily composed of rocks rich in clinopyroxene such as lherzolite, wehrlite and pyroxenite. Therefore, the occurrence of clinopyroxene is an important mineralogical indicator for the evolution of the lithospheric mantle from refractory to fertile.

The experimental results in this study show that the alkaline basaltic melt can consume orthopyroxene to form clinopyroxene under the temperature and pressure conditions of the lithospheric mantle, and most of the newly

formed clinopyroxenes are plotted in the range defined by the clinopyroxenes from the mantle lherzolites and pyroxenites in the NCC (Fig. 4), indicating that the reactions can transform harzburgites into lherzolites rich in clinopyroxene. The alkaline basaltic melt has higher CaO and Al_2O_3 contents than the orthopyroxene. As the melt reacts with the orthopyroxene to crystallize clinopyroxene, CaO and Al_2O_3 contents in the refractory mantle harzburgites increase accordingly, constructing a reaction or refertilization trend reported by Zhang (2009) and Tang et al. (2013), respectively.

It is worth noting that although the newly formed clinopyroxenes in this study, as above-mentioned and illustrated in Fig. 4, are plotted into the range defined by the clinopyroxenes in the mantle lherzolites and pyroxenites from the NCC, there is a certain deviation from the range defined by 95% of mantle clinopyroxenes. The main difference is that the component of Wo in the experimental clinopyroxenes is relatively lower. A recent summary from Wang et al. (2022) reveals that the CaO content in clinopyroxenes formed through the experimental reactions involving silicate melts is generally lower than that of some clinopyroxenes believed to be formed by metasomatism of silicate melts in the lithospheric mantle of the NCC. The results from our experiments in this study and summarized by Wang et al. (2022) suggest that if the formation of some metasomatic clinopyroxenes in the lithospheric mantle of the NCC is explained by the reactions between pure silicate melts and mantle rocks or minerals, the CaO content in the melts is insufficient. Consequently, the melts involved in the formation of these mantle clinopyroxenes are likely not pure silicate melts, but rather carbonated silicate melts rich in CaO.

4.3 Implication for genesis of basalts

Some researchers from case studies, based on petrographic and geochemical compositions of basalts, argued that melt-peridotite reactions could play an important role in formation and evolution of certain basalts. For example, formation of the Quaternary tholeiitic basalts from Datong, western NCC (Xu et al. 2005), generation of the EM1-type alkaline basalts in Payenia, Argentina (Søager and Holm 2013), genesis of the continental flood basalts in Tarim, NW China (Wang et al. 2023), evolution of the Datong basalts from alkaline to tholeiitic in western NCC (Wang and Liu 2021), and transition of the Karamay basalts from tholeiitic to alkaline in West Junggar, southern Central Asian Orogenic Belt (Xie et al. 2023). To verify these arguments, additional evidence, especially direct one from relevant experimental exploration, is required.

Several experiments of reaction between melt and rock or mineral under high-temperature and high-pressure conditions have been conducted to simulate the genesis of basalts. Wagner and Grove (1998) constrained the role of melt/harzburgite reaction in the petrogenesis of tholeiitic magma from Kilauea volcano in Hawaii based on experimentally determined results from the liquidus relations of an estimated primary tholeiite. Mallik and Dasgupta (2012) performed reaction experiments between eclogite-derived melts and fertile peridotite, and proposed that alkaline basalt and basanite from intraplate ocean islands could be generated by such reactions. Recently, Zang et al. (2021) reported the experimental results of reactions between tholeiitic melt and mantle orthopyroxene. The results indicate that the reactions might contribute to the generation of the ocean island basalts with high-SiO_2 in Hawaii and account for their chemical variability. These experimental investigations provide good direct evidence for the genesis of basalts. However, few experiments thus far have been conducted reactions between alkaline basaltic melt and mantle peridotite or mineral under high-temperature and high-pressure conditions.

In this study, the reacted melts of the reactions between the asthenosphere-derived alkaline basaltic melt and mantle orthopyroxene have varied major-element compositions to some extent compared to the starting melt (Table 3 and Fig. 3). As shown in Fig. 6, $Na_2O + K_2O$ contents in several reacted melts have obvious reduce due to dilution effect. Among ten runs in this study, the reacted melts in four ones (hq-12, 14, 15, 33) were transformed from the starting alkaline into subalkaline after reactions (Fig. 6), with Rittmann index (σ) not exceeding 1.8 (Table 3). In addition, except for run hq-12, the reacted melts in other

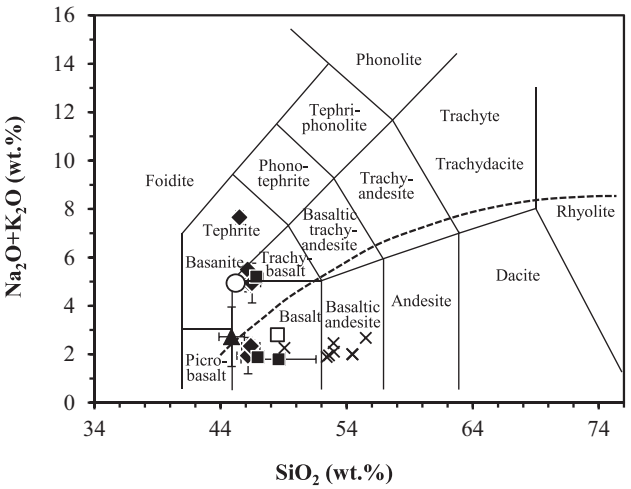

Fig. 6 The chemical classification and nomenclature of volcanic rocks using the total alkali-silica (TAS) diagram of Le Bas et al. (1986). The dashed line is the boundary between alkaline and subalkaline rocks from Miyashiro (1978). The unfilled square and cross are the starting and reacted melt from Zang et al. (2021), respectively. Other symbols are the same as those in Fig. 3

three ones are hypersthene-normative tholeiitic, indicating that the melts evolved into tholeiitic after reactions in these runs. Therefore, the experimental results in this study are of significance for the genesis of basalts, for example, providing key direct evidence for the evolution of the Datong basalts from alkaline to tholeiitic in Western NCC (Wang and Liu 2021).

5 Conclusions

1. Alkaline basaltic melts react with orthopyroxene under high-temperature and high-pressure conditions to form clinopyroxene. The formation of clinopyroxene in the reaction zone is mainly controlled by dissolution–crystallization, and the chemical composition of the reacted melt is primarily affected by diffusion effect.
2. Temperature is an important parameter for controlling the reaction between the melt and orthopyroxene. It directly affects the melting of orthopyroxene and the diffusion of chemical components in the melt, and constrains the chemical compositions of the newly formed clinopyroxene in the reaction zone and the reacted melt.
3. Alkaline basaltic melt originated from the asthenospheric mantle can consume orthopyroxene in the lithospheric mantle to form clinopyroxene. CaO and Al_2O_3 contents in the rocks are increased due to the occurrence of clinopyroxene. The reaction between alkaline basaltic melt and orthopyroxene can result in an evolution of the lithospheric mantle from refractory to fertile in the NCC.
4. The tholeiitic magma could be generated from alkaline basaltic one via reactions between the latter and orthopyroxene.

Acknowledgements This work was financially supported by the National Natural Science Foundation of China (Nos. 41472065 and 42073059). X. Li, W. Zheng, and B. Mo are appreciated for their assistance on the EPMA and SEM analysis. We thank W. Zhou, R. Li, and Y. Yin for their help on the experiments. We are very grateful to two anonymous reviewers for their constructive suggestions on improving the manuscript.

Author contributions The study of this paper was proposed and organized by HT. All the experiments and sample analysis were carried out by HH, who also prepared the original manuscript. MW provided experimental guidance. All authors improved the manuscript and contributed to interpretation of the results and geological implications.

Declarations

Conflict of interest The authors declare that there is no conflict of interest.

References

Bao ZA, He GF, Chen KY, Song JY, Yuan HL, Liu XM (2011) The primary development of glass rock standard by high temperature fusion: basalt as an example. Geochimica. 40(3):223–236 (**in Chinese with English abstract**).

Fan WM, Zhang HF, Baker J, Jarvis KE, Mason PRD, Menzies MA (2000) On and off the North China craton: Where is the Archaean keel? J Petrol. 41:933–950.

Gao S, Rudnick RL, Xu WL, Yuan HL, Liu YS, Walker RJ, Puchtel IS, Liu X, Huang H, Wang XR (2008) Recycling deep cratonic lithosphere and generation of intraplate magmatism in the North China Craton. Earth Planet Sci Lett. 270:41–53.

Gao S, Zhang JF, Xu WL, Liu YS (2009) Delamination and destruction of the North China Craton. Chin Sci Bull. 54:3367–3378.

Green TH (1982) Anatexis of mafic crust and high pressure crystallization of andesite. In: Thorpe RS (ed) Andesites. Wiley, New York, pp 465–487.

Kelemen PB, Joyce DB, Webster JD, Holloway JR (1990) Reaction between ultramafic rock and fractionating basaltic magma II. Experimental investigation of reaction between olivine tholeiite and harzburgite at 1150°C-1050°C and 5 kb. J Petrol. 31:99–134.

Le Bas MJ, Le Maitre RW, Streckeisen A, Zanettin B (1986) A chemical classification of volcanic rocks based on the total alkali-silica diagram. J Petrol. 27:745–750.

Liang Y (1999) Diffusive dissolution in ternary systems: analysis with applications to quartz and quartzite dissolution in molten silicates. Geochim Cosmochim Acta. 63(23):3983–3995.

Liang Y (2000) Dissolution in molten silicates: Effects of solid solution. Geochim Cosmochim Acta 64(9):1617–1627.

Liang Y (2010) Multicomponent diffusion in molten silicates: theory, experiments and geological applications. Rev Mineral Geochem. 72:409–446.

Liang Y, Richter FM, Davis AM, Watson EB (1996) Diffusion in silicate melts: self diffusion in $CaO–Al_2O_3–SiO_2$ at 1500℃ and 1 GPa. Geochim Cosmochim Acta. 60:4353–4367.

Liu ZC, Wu FY, Chu ZY, Xu XS (2010) Isotopic compositions of the peridotitic xenoliths from the Nushan area, Anhui Province: constraints on the age of subcontinental lithospheric mantle beneath the East China. Acta Petrol Sin. 26(4):1217–1240 (**in Chinese with English abstract**).

Lu FX (2010) Multiple-geological events of ancient lithospheric mantle beneath North China Craton: As inferred from peridotite xenoliths in kimberlite. Acta Petrol Sin. 26(11):3177–3188 (**in Chinese with English abstract**).

Mallik A, Dasgupta R (2012) Reaction between MORB-eclogite derived melts and fertile peridotite and generation of ocean island basalts. Earth Planet Sci Lett. 329–330:97–108.

Miyashiro A (1978) Nature of alkali volcanic rock series. Contrib Mineral Petrol. 66:91–104.

Morgan Z, Liang Y (2003). An experimental and numerical study of the kinetics of harzburgite reactive dissolution with applications to dunite dike formation. Earth Planet Sci Lett. 214:59–74.

Morgan Z, Liang Y (2005). An experimental study of the kinetics of lherzolite reactive dissolution with applications to melt channel formation. Contrib Mineral Petrol. 150:369–385.

Ravna EK (2000) The garnet-clinopyroxene geothermometer–an updated calibration. J Metamorphic Geol. 18:211–219.

Sisson TW, Grove TL (1993) Experimental investigations of the role of H_2O in calc-alkaline differentiation and subduction zone magmatism. Contrib Mineral Petrol. 113:143–166.

Søager N, Holm PM (2013) Melt–peridotite reactions in upwelling eclogite bodies: constraints from EM1-type alkaline basalts in Payenia, Argentina. Chem Geol. 360–361:204–219.

Sun J, Liu CZ, Wu FY, Yang YH, Chu ZY (2012) Metasomatic origin of clinopyroxene in Archean mantle xenoliths from Hebi, North China Craton: trace-element and Sr-isotope constraints. Chem Geol. 328(11):123–136.

Tang YJ, Zhang HF, Ying JF, Su BX (2013) Widespread refertilization of cratonic and circum-cratonic lithospheric mantle. Earth Sci Rev. 118:45–68.

Wagner TP, Grove TL (1998) Melt/Harzburgite reaction in the petrogenesis of tholeiitic magma from Kilauea volcano. Hawaii Contrib Mineral Petrol. 131:1–12.

Wang ZZ, Liu SA (2021) Evolution of intraplate alkaline to tholeiitic basalts via interaction between carbonated melt and lithospheric mantle. J Petrol. 62:egab025.

Wang ML, Tang HF (2013) Reaction experiments between tonalitic melt and mantle olivine and their implications for genesis of high-Mg andesites within cratons. Sci China Earth Sci. 56:1918–1925.

Wang CG, Liang Y, Xu WL, Dygert N (2013) Effect of melt composition on basalt and peridotite interaction: laboratory dissolution experiments with applications to mineral compositional variations in mantle xenoliths from the North China Craton. Contrib Mineral Petrol. 166:1469–1488.

Wang ML, Zang CJ, Tang HF (2019) The effect of P-T on the reaction between tonalitic melt and mantle lherzolite at 2–4 GPa and implications for evolution of North China Cratonic lithosphere and generation of high Mg# andesite. Lithos. 324–325:626–639.

Wang CG, Lo Cascio M, Liang Y, Xu WL (2020) An experimental study of peridotite dissolution in eclogite-derived melts: Implications for styles of melt-rock interaction in lithospheric mantle beneath the North China Craton. Geochim Cosmochim Acta. 278:157–176.

Wang XF, Zhang JF, Wang C, Zong KQ, Xu HJ (2022) Experimental constraint on Ca-rich carbonatite melt-peridotite interaction and implications for lithospheric mantle modification beneath the North China Craton. J Geophys Res Solid Earth. 127:e2022JB024769.

Wang ZC, Zhang ZC, Reichow MK, Tian W, Kong WL, Liu BX (2023) Tracing decarbonated eclogite in the mantle sources of Tarim continental flood basalts using Zn isotopes. GSA Bull. 135:1768–1782.

Wu FY, Xu YG, Gao S, Zheng JP (2008) Lithospheric thinning and destruction of the North China Craton. Acta Petrol Sin. 24(6):1145–1174 (**in Chinese with English abstract**).

Wyllie PJ (1979) Magmas and volatile components. Am Mineral. 64:469–500.

Xiao Y, Zhang HF, Fan WM, Ying JF, Zhang J, Zhao XM, Su BX (2010) Evolution of lithospheric mantle beneath the Tan-Lu fault zone, eastern North China Craton: Evidence from petrology and geochemistry of peridotite xenoliths. Lithos. 117:229–246.

Xiao Y, Zhang HF, Deloule E, Su BX, Tang YJ, Sakyi PA, Hu Y, Ying JF (2015) Large lithium isotopic variations in minerals from peridotite xenoliths from the eastern North China Craton. J Geol. 123:79–94.

Xie QH, Zhang ZC, Foley SF, Chen CF, Cheng ZG, Wang Y, Kong WL, Lv YW, Santosh M, Jin QZ, Krmíček L, Zhu XK (2023) Transition from tholeiitic to alkali basalts via interaction between decarbonated eclogite-derived melts and peridotite. Chem Geol. 621:121354.

Xu YG (2001) Thermo–tectonic destruction of the Archaean lithospheric keel beneath the sino-korean craton in China evidence, timing and mechanism. Phys Chem Earth A. 26:747–757.

Xu YG, Ma JL, Frey FA, Feigenson MD, Liu JF (2005) Role of lithosphere–asthenosphere interaction in the genesis of Quaternary alkali and tholeiitic basalts from Datong, western North China Craton. Chem Geol. 224:247–271.

Yaxley GM, Green DH (1998) Reactions between eclogite and peridotite: mantle refertilisation by subduction of oceanic crust. Schweiz Mineral Petrogr Mitt. 78:243–255.

Yu CM (2009) Ages of peridotitic xenoliths from central and eastern areas of North China Craton and mantle heterogeneity. Dissertation, China University of Geosciences **(in Chinese with English abstract).**

Zang CJ, Wang ML, Tang HF, He HQ (2021) Reaction between basaltic melt and orthopyroxene at 3.0–4.5 GPa: Implications for the evolution of ocean island basalts in the mantle. Geosci Front. 12:907–919.

Zhang HF (2006) Peridotite-melt interaction: an important mechanism for the compositional transformation of lithospheric mantle. Earth Sci Front. 13(2):65–75 (**in Chinese with English abstract**).

Zhang HF (2009) Peridotite-melt interaction: a key point for the destruction of cratonic lithospheric mantle. Chin Sci Bull. 54:3417–3437.

Zhang HF, Zheng JP (2003) Geochemical characteristics and petrogenesis of Mesozoic basalts from the North China Craton: A case study in Fuxin, Liaoning Province. Chin Sci Bull. 48:924–930.

Zhang HF, Nakamura E, Kobayashi K, Kobayashi K, Zhang J, Ying JF, Tang YJ, Niu LF (2007) Transformation of the subcontinental lithospheric mantle through deformation–enhanced peridotite-melt reaction: Evidence from a highly fertile mantle xenolith from the North China Craton. Int Geol Rev. 49:658–679.

Zheng JP (2009) Comparison of mantle-derived matierals from different spatiotemporal settings: Implications for destructive and accretional processes of the North China Craton. Chin Sci Bull 54:3397–3416.

Zheng JP, Lu F, O'Reilly SY, Griffin WL, Zhang M (2000) Mantle modification and replacement in eastern North China: Laser probe study on clinopyroxene. Sci China (ser d). 30(4):373–382 (**in Chinese**).

Zheng JP, Griffin WL, O'Reilly SY, Liou JG, Zhang RY, Lu FX (2005) Late Mesozoic-Eocene mantle replacement beneath the eastern North China Craton: Evidence from the Paleozoic and Cenozoic peridotite xenoliths. Int Geol Rev. 47(5):457–472.

Zheng JP, Lu FX, Griffin WL, Yu CM, Zhang RS, Yuan XP, Wu XL (2006a) Lithospheric thinning accompanying mantle lateral spreading, erosion and replacement beneath the eastern part of North China: Evidence from peridotites. Earth Sci Front. 13(2):076–085 (**in Chinese with English abstract**).

Zheng JP, Griffin WL, O'Reilly SY, Yang JS, Li TF, Zhang M, Zhang RY, Liou JG (2006b) Mineral chemistry of peridotites from Paleozoic, Mesozoic and Cenozoic lithosphere: constraints on mantle evolution beneath eastern China. J Petrol. 47(11):2233–2256.

Zheng JP, Yu CM, Lu FX, Zhang ZH (2007a) Age and composition of continental mantle peridotites and implications for the lithospheric thinning, eastern North China. Earth Sci Front. 14(2):87–97 (**in Chinese with English abstract**).

Zheng JP, Griffin WL, O'Reilly SY, Yu CM, Zhang HF, Pearson N, Zhang M (2007b) Mechanism and timing of lithospheric modification and replacement beneath the eastern North China Craton: peridotitic xenoliths from the 100 Ma Fuxin basalts and a regional synthesis. Geochim Cosmochim Acta. 71(21):5203–5225.

Zhou XH (2006) Major transformation of the subcontinental lithosphere beneath eastern China in the Cenozoic–Mesozoic: Review and prospect. Earth Sci Front. 13(2):50–64 (**in Chinese with English abstract**).

Zou DY (2010) Transformation of the lithospheric mantle through peridotite-melt interaction: Evidence from the mantle xenoliths in the northern margin of the North China Craton. Dissertation, Northwest University **(in Chinese with English abstract).**